How unique is unique? Quantifying geometric differences in stripe patterns of Cape mountain zebra, *Equus zebra zebra* (Perissodactyla: Equidae)

By Nicolas D **Prinsloo***; Martin Postma and P J Nico de Bruyn

Mammal Research Institute, Department of Zoology and Entomology, University of Pretoria, Private Bag X20, Hatfield 0028, South Africa

* Corresponding author. E-mail: nicolas.prinsloo7@gmail.com

Abstract

Quantified coat pattern dissimilarity provides a visible surface for individual animal traceability to populations. We determined the feasibility in quantifying uniqueness of stripe patterns of Cape mountain zebra (CMZ; *Equus zebra zebra*) using geometric morphometrics. We photogrammetrically created dense surface models of CMZ (N =56). Stripe edges were landmarked, superimposed and compared for shape variation across replicates and the population. Significant allometry in stripe patterns prompted allometric correction to remove increased curvature of stripes at the rump, belly and back with larger adult individuals, to facilitate equilibrated comparison between individuals. Re-landmarked replicates showed lower dissimilarity (D_i) than non-replicates (D_p), representing minimal landmarking error. Individuals were 78.07±1.79% unique ($U = 1 - \frac{D_i}{D_p} \times 100\%$) relative to the study population. Size, the number of torso stripes and degree of branching in four rear torso stripes described the most shape variation (36.79%) but a significant portion could only be distinguished with geometric morphometrics (41.82%). This is the first known use of geometric morphometrics to quantify coat pattern uniqueness, using a model species to provide baseline individual morphological variation. Measures of coat pattern similarity have a place in phenotypic monitoring and identification.

Keywords: coat patterns; geometric morphometrics; heat maps; morphological variation; pattern variation; photogrammetry; shape variation

INTRODUCTION

Patterns biologically printed across some animal surfaces are frequently used for identification (Penzhorn, 1984; Kelly, 2001; Hiby *et al.*, 2009). However, human bias is retained in qualitative distinctions. Quantifying coat pattern variation would refine identification efficiency and accuracy by addition of 'how different' to 'two individuals are different'. Quantified morphological differences sometimes correlate to equally informative genetic (Bandeira *et al.*, 2017) or ecological differences (Davis *et al.*, 2016). Sets of external morphological traits are characteristic to geographic regions (Bandeira *et al.*, 2017) or populations (Vendrami *et al.*, 2017) and help distinguish between species (Purroy *et al.*, 2016). Refined individual identification and measures of morphological difference are necessary for animal tracking and monitoring for disease control (Tharwat *et al.*, 2017), population counts, behavioural, demographic and ecological research (Penzhorn, 1984;

Penzhorn & Novellie, 1991; Norouzzadeh *et al.*, 2018), systematics, phenotypic monitoring and conservation (Wisely *et al.*, 2008).

Previous efforts to quantify differences in coat pattern (for identification) used 2D images overlaid onto generic 3D models (Kelly, 2001; Hiby *et al.*, 2009) and feature extraction (Crall *et al.*, 2013; Tharwat *et al.*, 2017). With enough training, machine and deep-learning models are also able to identify individuals based on their characteristic coat patterns (Cheema & Anand, 2017). Given their broad-scale applicability to images of varying quality from voluminous citizen data (Mason, 2016), there is no standardized data collection. These methods allowed for individual matching of animals photographed at varying distances, in different orientations or postures. However, the size dimensions of the growing animals are not known nor treated dynamically. Although these approaches achieve high recognition rates for animals at a given life stage, it is uncertain how this is affected over time with growth or changes in condition. Other methods included codes for variable characters (Peterson, 1972; Miththapala *et al.*, 1989). Resulting dissimilarity indices are precise for recognition but may be inaccurate or skewed for morphological variation.

Three-dimensional photogrammetry and geometric morphometrics can account for different positions, sizes, orientations and allometric shape changes (Gower, 1975). Geometric characterization of many anatomical components across varying species has provided insight into their evolutionary history (Purroy *et al.*, 2016), current diversity (Bignon *et al.*, 2005; Vendrami *et al.*, 2016), ecology (Jansky *et al.*, 2013; Schmieder *et al.*, 2015) and conservation concerns (Marquez *et al.*, 2010; McGuire, 2011; Luceño *et al.*, 2013). Computational complexity hitherto probably limited the use of geometric morphometrics for pattern variation, specifically its application to patterns across a 3D surface (McGuire, 2011). Furthermore, not associating 3D photogrammetry with geometric morphometric application for whole, large, terrestrial mammals, has hampered insights into quantified condition (Henneke, 2011), skin cell expansion and cell migration (Yamaguchi *et al.*, 2007).

Zebra stripes present a useful contrasting striped surface to estimate pattern variation within and between populations. Unlike most other striped mammals, zebra stripes are well defined; simplifying the geometric morphometric approach. Additionally, zebras are highly symmetrical (72% to 83%; Reddy & Aravind, 2012). Mountain zebras (*Equus zebra* Linnaeus, 1758) have intermediately thick and sparse stripes that rarely reach the ventral midline, which reduces the coverage required to model the stripe patterns. Uniquely, mountain zebras have a grid-iron pattern above the rump (Penzhorn, 1988; Groves & Bell, 2004).

Hartmann's (*E. z. hartmannae* Matschie, 1898) and Cape (*E. z. zebra*) mountain zebra (HMZ and CMZ, respectively) are qualitatively distinguished by minor differences in stripe pattern. CMZ rump stripes are more closely spaced and torso stripes sometimes reach around the chest (Novellie *et al.*, 2002; Groves & Bell, 2004). These observations are relative and as such there is little confidence attributed to pattern differences between the mountain zebra subspecies. Observers often relied on CMZ being smaller than HMZ, with a mane that does not extend as far forward (Novellie *et al.*, 2002). HMZ are often translocated into CMZ distribution, resulting in their hybridization (Hrabar *et al.*, 2016). Accurate quantitative distinction between populations of HMZ and CMZ may prevent their sympatry, help determine the origin of the incorrectly translocated individuals and detect hybrids, which are difficult to detect qualitatively (Hrabar *et al.*, 2016). Furthermore, individual identification of CMZ in long-term behavioural studies relied on qualitative stripe pattern uniqueness

(Penzhorn, 1984; Penzhorn & Novellie, 1991). Quantification of pattern variation would prove useful but, first, baseline pattern variation needs to be established.

We hypothesized that 3D modelling and geometric morphometrics can consistently quantify pattern variation of individuals. In our effort to assess how unique is unique, our main objectives were to: (1) determine the methodology and feasibility in quantifying CMZ stripe pattern uniqueness using geometric morphometrics, (2) recognize variable stripe features that are useful for identification and (3) develop a baseline for CMZ stripe pattern variation. We expect low resampling error, geometrically unique individuals and variable torso stripes where branching occurs.

MATERIAL AND METHODS

Photogrammetry

In May 2016, Mountain Zebra National Park (MZNP) management herded CMZ into an enclosure prior to translocation. Associated with capture procedures, all individuals were chemically immobilized to test for possible hybridization (parallel genetic studies; Dalton *et al.*, 2017a). Individuals were sexed and grouped into age classes. While sedated, we photographed the sides of zebra bodies with either an array of four calibrated GoPro Hero4 Silver 3 (see S1) or a calibrated Canon EOS 400D at set focal lengths (3 mm and 18 mm, respectively) taking enough overlapping photos (~24) (minimum = 16) of each individual from different angles with the zebra filling the field of view to provide sufficient 3D coverage. Prior to data capture, we calibrated cameras as set out by Photomodeler Scanner guidelines (EOS Systems Inc).

Calibrations (as above) were assigned to cameras in each photogrammetric scan. A SmartPoints (Photomodeler Scanner 2018.0.1.2245) function automatically marked common features at the highest point density and oriented the photographs within the 3D space. Dense surface modelling with triangulation simulated the photographed surface; environmental surface was removed. Models with mismatched textures were realigned in MeshLab (Cignoni *et al.*, 2008). Dense surface models of three subadult colts, three subadult fillies, 17 juveniles, 27 mares and six stallions (N = 56) were retained for further analysis. We measured project accuracy by assessing the range of maximum residuals (2.1 to 4.3 pixels) against the recommended upper limit of five pixels (see Photomodeler Scanner help file).

Geometric morphometrics

We focused on the three rump (R1–3) and rear nine torso stripes (back-to-front) (T1–9) as they were homologous among individuals in the study and covered a broad region of the body (Fig. 1). Some stripes barely extended half-way down the side, were non-homologous and thus excluded from landmarking (half-stripes). The grid-iron pattern was enveloped in the uppermost rump stripe. We placed subjective landmarks on each stripe edge for a subset of individuals. After removing outliers, we used the upper confidence limits of landmark numbers to avoid under-description of stripe shape for each edge (Fig. 2). Within R (R Core Team, 2018), we compared landmark numbers between stripe edges using a pairwise *t*-test and assigned mode upper confidence limits to landmark numbers for similar stripe edges (Table 1; total landmarks = 209).

Table 1. The significance of differences between each stripe edge and following stripe edges (pairwise *t*-test) from back (B) to front (F). Sets of landmarks (mean + 2 SD) were assigned to each stripe with significant differences (*; $P < 0.05$) from all following stripe edges, otherwise the mode mean + 2 SD ($_a$) landmark number of following stripes was used for that stripe edge

Stripe	#	Edge	*P*-value	Landmarks
Rump*	1*	B	<0.01	10
		F	<0.01	12
	2*	B	<0.01	13
		F	<0.01	16
	3*	B	<0.01	14
		F	<0.01	13
Torso	1*	B	<0.01	12
		F	<0.01	13
	2*	B	0.03	12
		F	0.03	12
	3	B	1	11_a
		F	1	11_a
	4	B	1	11_a
		F	1	11_a
	5	B	1	11_a
		F	1	11_a
	6	B	1	11_a
		F	1	11_a
	7	B	1	11_a
		F	1	11_a
	8	B	1	11_a
		F	1	11_a
	9	B	1	11_a
		F	1	11_a

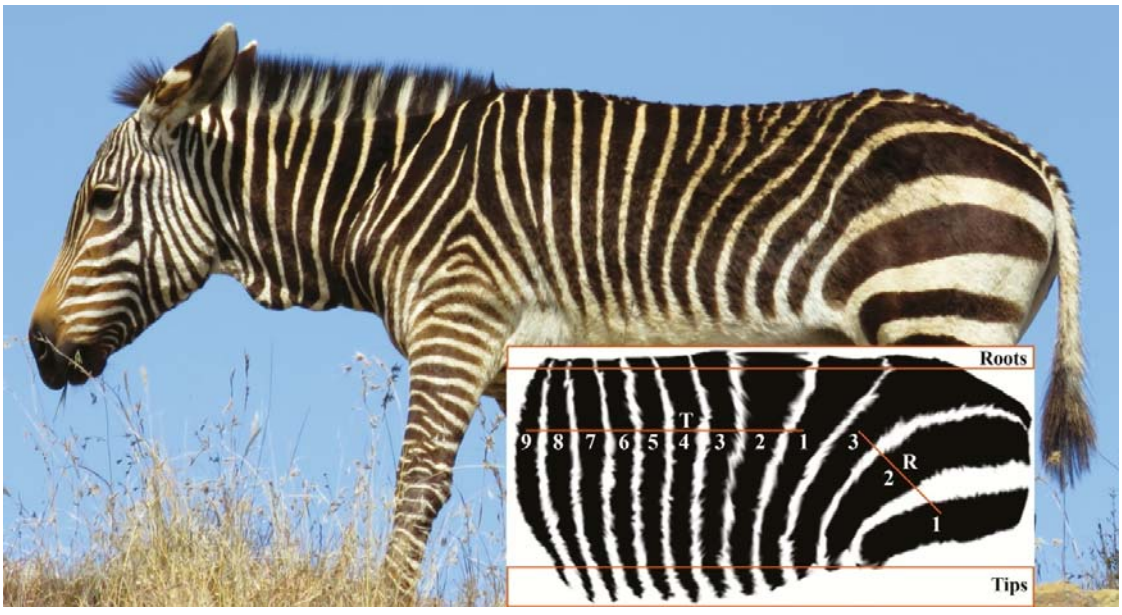

Figure 1. Image of a Cape mountain zebra, *Equus zebra zebra* (Perissodactyla: Equidae). Inset: a mean-shaped reference model with stripe names. Torso stripes (T1–9) are rooted at the dorsal midline with tips reaching the abdomen. Rump stripes (R1–3) have at least one edge that tends towards the rectum; R1 and R2 are tipped at their upper end, while R3 envelopes the grid-iron pattern. All lower rump stripe tips occur near the groin. The references model had branches and half-stripes removed, and contrast increased.

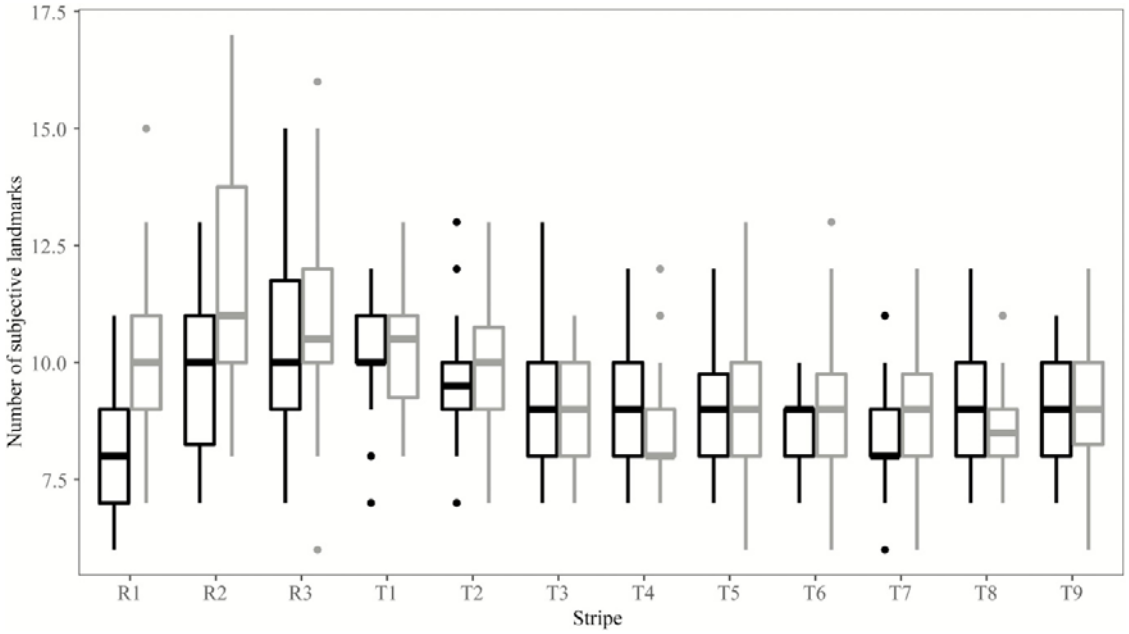

Figure 2. Variation in subjectively placed landmarks to describe the shape of each stripe. The number of landmarks for rump stripes (R1–3) are followed by torso stripes (T1–9). Black boxes represent the rear edges, and grey boxes represent the front edges. Median (bold horizontal bar), quartiles (thin horizontal bars) and extra-quartile values (single vertical bars) of the number of subjectively placed landmarks are represented. Outliers (dots) were removed before determining the minimum number of landmarks required to describe stripe shapes (mean + 2 SD).

Landmark configurations describing the overall shapes of the rump and rear nine torso stripes were digitized from rear to front in Landmark (Wiley *et al*., 2005) and imported into R as *.pts* files for geometric morphometrics and further statistical analyses. We assigned fixed (roots and tips of stripes) or semi-sliding functions (stripe edges) to landmarks using the *geomorph* package (Adams & Otárola-Castillo, 2013). Procrustes relaxation minimized distances between corresponding edges across individuals by iteratively fixing semi-sliding landmarks and sliding corresponding landmarks along tangent vectors between fixed landmarks (Adams & Otárola-Castillo, 2013).

Using a generalized Procrustes analysis (GPA; converged at six iterations), we only considered stripe pattern variation. The GPA calculated centres for landmark configurations ($\bar{x}, \bar{y}$ and $\bar{z}$), which it translated to the origin (0,0,0) by moving each landmark around the origin ($x_1 - \bar{x}, y_1 - \bar{y}$ and $z_1 - \bar{z} \cdots z_k - \bar{z}$) (Gower, 1975). The GPA calculated a size coefficient or centroid size (*s*) from the root mean square distance of the landmarks to the origin, corrected for the number of landmarks (*k*) (Gower, 1975):

$$s = \sqrt{\frac{(x_1 - \bar{x})^2 + (y_1 + \bar{y})^2 + (z_1 + \bar{z})^2}{k}}$$

Landmark configurations were rescaled by their corresponding size coefficients and rotated to further minimize the sum of squared distances between corresponding points.

In a pairwise manner, we calculated Procrustes distance (*d*; a measure of dissimilarity) as the square-rooted sum of squared distances between corresponding landmarks on each individual and replicate (Bookstein, 1996):

$$d = \sqrt{\sum_{n=1}^{k=269} (x_1 - x_2)^2 + (y_1 - y_2)^2 + (z_1 - z_2)^2}$$

Individuals were coordinated within a multidimensional morphospace separated by Procrustes distance. Using principal component analysis, we reduced dimensionality of the morphospace to 49 principal components (PCs) that described 99% of the shape variation. A number appended to PC represented different principal components.

Conventionally, studies use thin-plate splines to illustrate shape changes along principal components (Adams & Otárola-Castillo, 2013). However, bodily stripe patterns are too complex to be well represented on thin-plate splines. Instead, we developed a reference model by removing branches, overlaying landmarks and warping it to represent the mean stripe pattern. The reference model was distorted to represent patterns at minimum and maximum values along PCs, which we superimposed to calculate the distances between corresponding vertices. RGB values are red, green and blue values (0-255) combined to compute colour. Where the top 10%, 5% and 1% of shape variation occurred, we increased the red values (100, 200 and 255, respectively) on the reference model. Thus, the readability of complex changes in surface patterns was improved (Fig. 3). Colourized models were warped 50 times along principal components to animate stripe changes as Graphics Interchange Format images (GIFs; see S2).

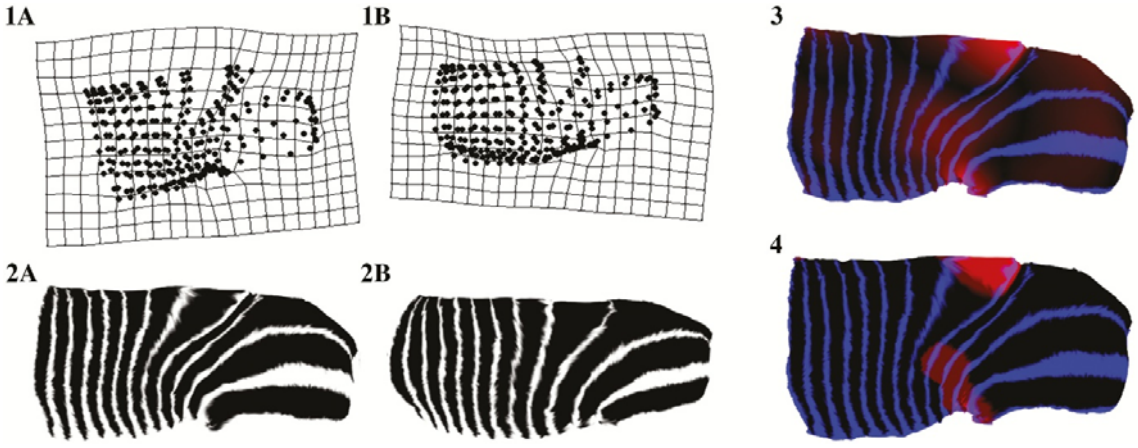

Figure 3. The progression from conventional geometric morphometric visualizations to heat maps. Stripe difference from min (A) to max (B) along PC1, prior to allometric correction, are illustrated as traditional thin-plate splines (1) and warped models (*geomorph*) (2). Distances between corresponding vertices on the warped models were calculated and colourized on a single model (3). Redness on the model, warped for minimum values of the principal component, highlights stripes and stripe components with shape change along the principal axis. Thresholds were set to the top 1%, 5% and 10% of vertex movement with geometric changes along the principal axes, and colourized as RGB redness (255, 200 and 100, respectively) (4).

We recorded the degree of branching for each torso stripe, presence or degree of branching of half-stripes, size and the number of torso stripes as variables measurable without geometric morphometrics, i.e. non-geometric traits. Contrastingly, geometric traits were only feasibly measured with geometric morphometrics, including curvature, branch shape, tip pointedness or roundness, etc. The relationship between overall stripe pattern, size and the number of torso stripes was determined using allometric and Procrustes regression (999 iterations). Additionally, principal components were regressed with non-geometric traits. Regression models for each PC began with variables that, when used alone, were significantly related to PCs ($P > 0.1$) (Fisher, 1926). Thereafter, we included or excluded interactions or variables from models until reaching the lowest Akaike Information Criterion corrected for small sample size (AICc). If the non-geometric variables did not predict shape represented along principal components, then random variables (represented by 1) were considered and geometric traits better described shape variation along these PCs. If models did not meet the assumptions of normality of variance, linearity, homoscedasticity and no kurtosis, tested using *gvlma* package (Peña & Slate, 2006), then these models were ignored as the effects were expected to be linear along principal components. In a full model, we included all non-geometric traits to determine their independent effects on stripe pattern using Procrustes regression. Thereafter, allometry was corrected using aligned coordinates residual to the allometric relationship.

We produced a consensus tree (bootstraps = 10000) [*agricolae* package (de Mendiburu, 2017)] based on posterior Procrustes distances. Various clustering algorithms (*complete*, *single*, *ward.D*, *ward.D2*, *average*, *mcquitty*, *median* and *centroid*) were compared to determine whether replicates were reassigned to the correct individual based on their PC values.

We developed a uniqueness index, where U is the uniqueness of individuals; d_i is the Procrustes distance between re-landmarked replicates and d_p is the Procrustes distance between individuals in the population:

$$U = 1 - \frac{d_i}{d_p} \times 100\ \%$$

Markov chain Monte Carlo (MCMC) methods randomly sampled Procrustes distances from posterior distributions for each category and produced a distribution of possible uniqueness values (confidence interval = 95%). If dissimilarity of the population d_p was high and re-landmarked replicates d_i was low, then the uniqueness U tended towards 100%. If dissimilarity within the population was low and re-landmarked replicates was high, then the uniqueness tended towards 0%; suggesting too many shared geometric traits or high sampling error and unreliable identification by the method. We set a cut-off for hypothesis testing (U_T=50%) and calculated individual uniqueness.

RESULTS

Allometry and stripe features

Torso stripe number varies among individuals, from nine to 12. Shape is weakly related to torso stripe number ($F_{1,54} = 3.8$; $R^2 = 0.07$; $P = 0.001$). More torso stripes translate to narrower stripes with less branching; more horizontally compact. The seventh to ninth torso stripes are rounder, filling the space above the front shoulder in individuals with fewer stripes

(Fig. 4). Principal component 1 ($F_{1,54}$ = 11.9; R^2 = 0.18; P = 0.001), PC3 ($F_{1,54}$ = 7.7; R^2 = 0.12; P = 0.008), PC4 ($F_{1,54}$ = 5.3; R^2 = 0.09; P = 0.026) and PC5 ($F_{1,54}$ = 8.9; R^2 = 0.14; P = 0.004) are related to the number of torso stripes.

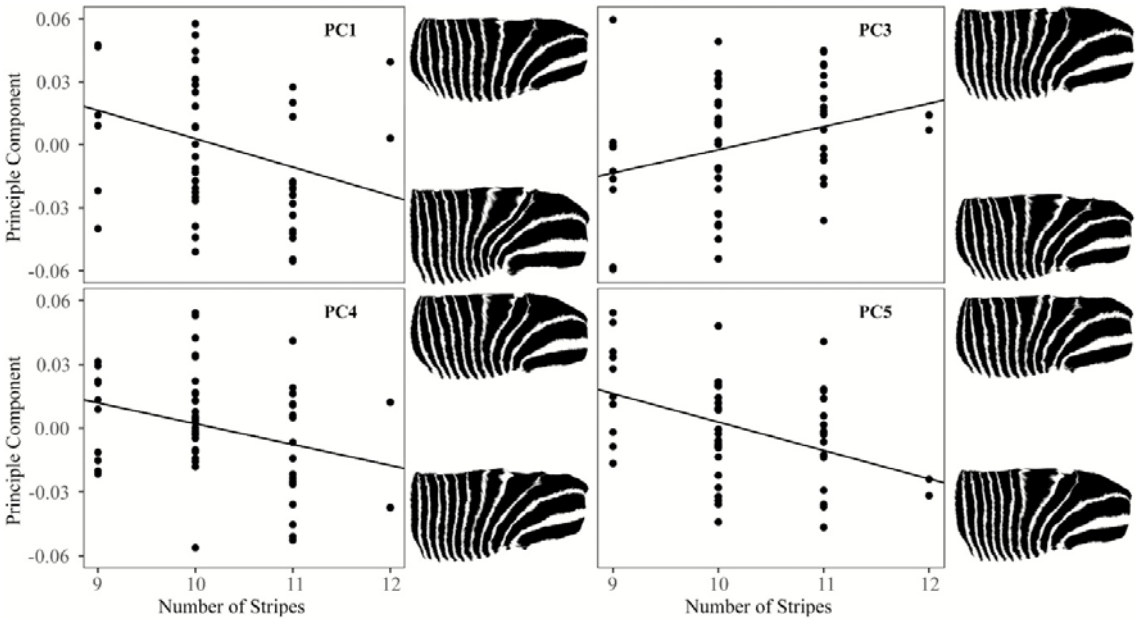

Figure 4. The influence of the number of torso stripes on shape via: PC1, PC3, PC4 and PC5. The most likely effect of decreasing stripe number is rounding of the front stripes (T7–9) above the shoulder, and widening of the stripes. Illustrated using warped models (*geomorph*).

Allometry is weakly supported ($F_{1,51}$ = 7.8; R^2 = 0.13; P = 0.001). Larger individuals have rounder abdomens, rumps and lower backs that affect stripe patterning (Fig. 5). Principal component 1 ($F_{1,54}$ = 46.6; R^2 = 0.46; P < 0.001), PC2 ($F_{1,54}$ = 12.5; R^2 = 0.19; P < 0.001), PC3 ($F_{1,54}$ = 3.3; R^2 = 0.06; P = 0.07), PC5 ($F_{1,54}$ = 2.9; R^2 = 0.05; P = 0.09) and PC8 ($F_{1,54}$ = 4.8; R^2 = 0.08; P = 0.03; Fig. 6) are allometric.

Figure 5. The allometric effect on stripe pattern illustrated using warped models (*geomorph*). Heat maps are plotted on models warped to illustrate minimum size. RGB redness (255, 200, 100) has been constrained to regions with the top 1%, 5% and 10% of allometric shape variation, respectively. From smaller (1A) to larger individuals (1B), the body tends to fill the ectoderm resulting in a much rounder lateral abdomen, rump and lower back (2).

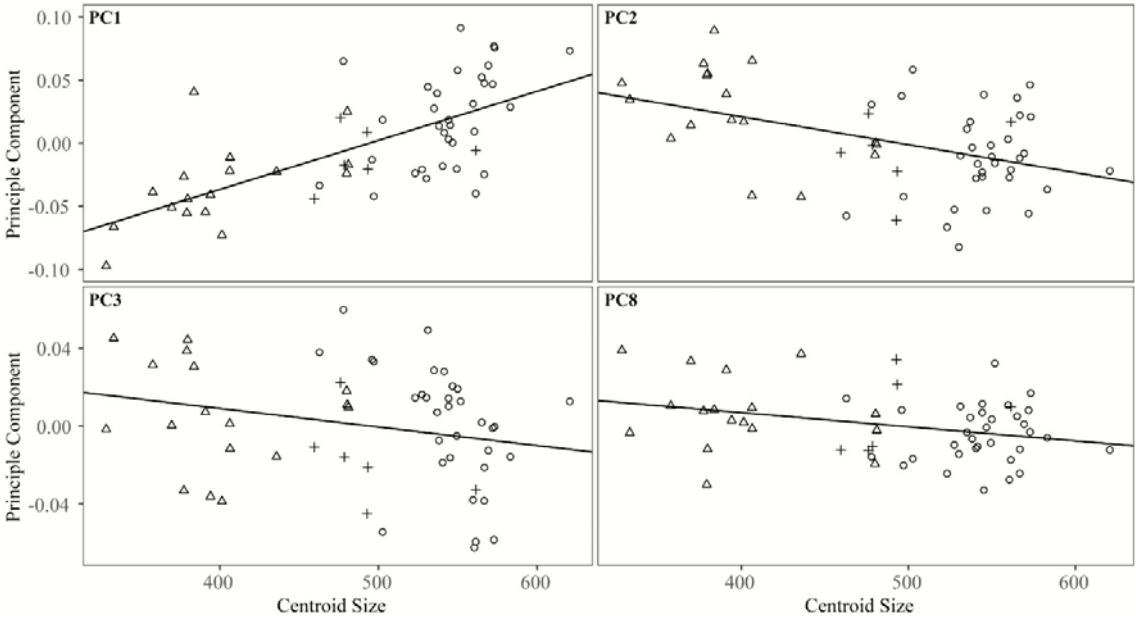

Figure 6. Significant allometric relationships with PC1, PC2, PC3 and PC8. As expected, juveniles (triangles), subadults (crosses) and adults (circles) cluster along the axis of centroid size, with some overlap.

The most parsimonious models from stepwise selection identified significant branching and changes in half-stripes along different principal components, while accounting for differences in size or number of torso stripes (see Appendix 1). The first torso stripe broadens and branches with increased PC1 (see Appendix 2). PC1, PC2 and PC3 explain 18.81%, 15.00% and 9.06% of the shape variation, accumulating 42.87% of the shape variation.

Allometry explains the most pattern variation (12.79%), followed by branching of the first three torso stripes and torso stripe number (Table 2). More than half of the shape variation (58.18%) is explained outside of the geometric morphometric framework. Importantly, the 41.82% shape variation explained with the geometric morphometric approach improves comparison of individuals, including curvature of stripes, pointedness or roundness of stripe tips, branch shape and various aspects of the rump stripes that we could not feasibly measure otherwise (Fig. 7).

Table 2. Procrustes variation explained by alternatively measurable features. These features include: counted number of branches in torso stripes, half-stripes and their degree of branching in front of the grid-iron pattern or in front of torso stripes, the number of torso stripes and size (allometry). Landmark coordination is the response variable within a Procrustes regression. These variables were placed in a single model and explanatory power may depend on information that has already been explained. We calculated a percentage (%) of the total variation (Σ) explained by each variable. Residual variation represents shape variation that cannot be explained by these features, including: curvature of stripes, pointedness or roundness, various aspects of the rump stripes, branch shape, etc.

Feature	Torso Stripes	Explained Variation
Size (allometry)		12.79%
Number of torso stripes		4.27%
Branching in torso stripes	1	7.13%
	3	5.37%
	2	4.86%
	4	2.37%
	7	1.91%
	5	1.82%
	6	1.46%
	8	1.10%
	9	0.56%
Absence or branching in half-stripes between torso stripes or grid-iron pattern (G)	G-1	3.50%
	7–8	2.00%
	5–6	1.81%
	2–3	1.73%
	8–9	1.63%
	1–2	1.52%
	6–7	1.29%
	3–4	1.06%
Σ		58.18%
Residual		41.82%

Figure 7. Heat map showing the accumulated pattern variation for each PC (see Appendix Figure), weighted for the importance of each PC. The degree of redness indicates areas of the highest pattern variation. Branching of the first four torso stripes and allometric aspects are confirmed to be important (Table 2).

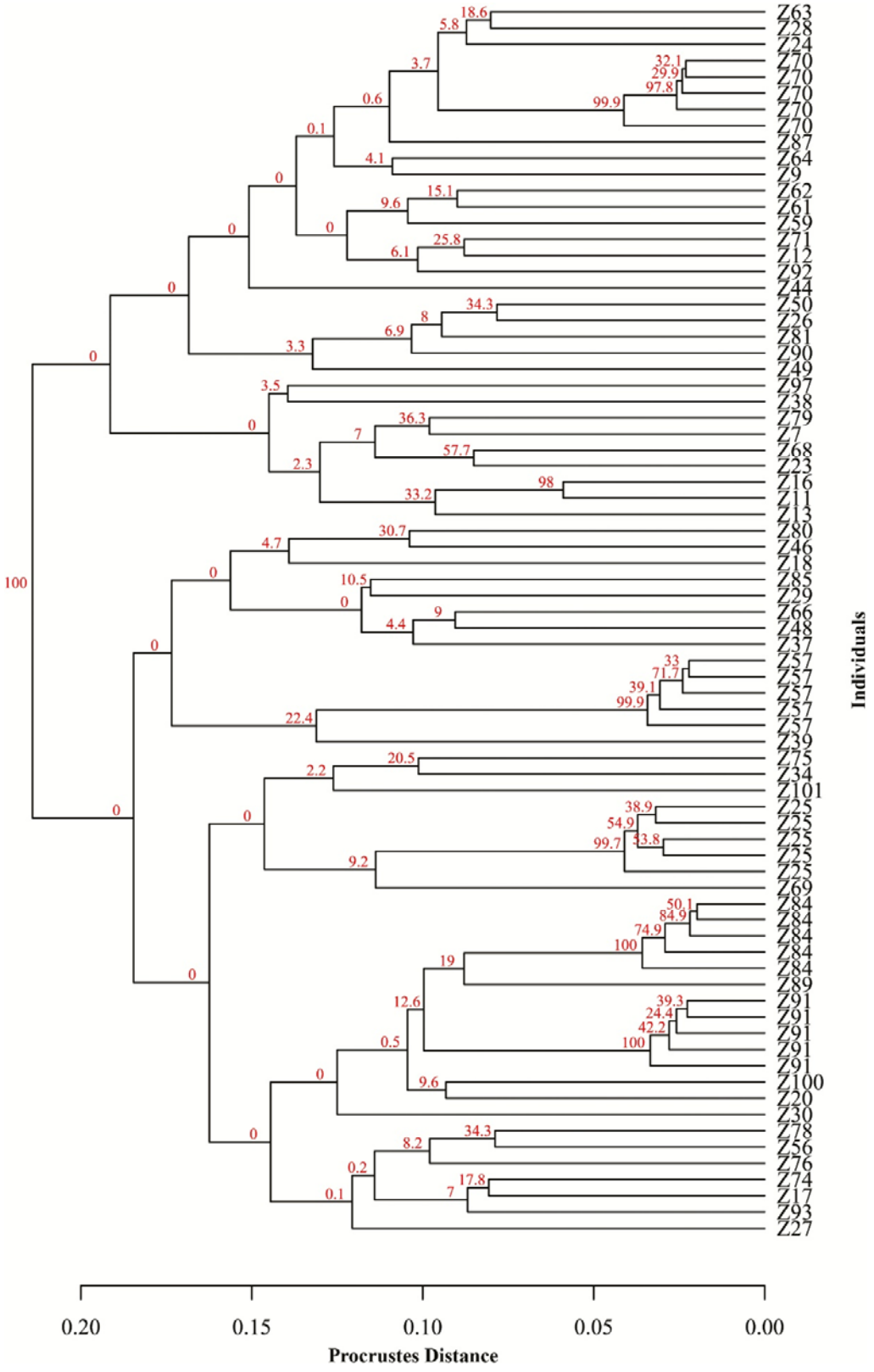

Figure 8. Clustering of re-landmarked replicates in a dendrogram (k = 56; bootstrap N = 10000) with the lowest Procrustes distances and high bootstrap support (red numbers at nodes) between replicates.

Uniqueness

Cluster analysis of individual replicates has bootstrap support ($\bar{b}$) for replicate clusters with ranges 25–100 ($\bar{b}$ = 66.7) and 0–58 ($\bar{b}$ = 11.7) for non-replicates (Fig. 8). The best clustering algorithm is *ward.D2*, reassigning replicates to the same individuals with 100% accuracy, precision, sensitivity and specificity. However, it reaches 15.91% precision and 10.14% sensitivity in reassigning individuals to correct groups; no better than randomly assigned groups with 6.82% precision and 6.67% sensitivity. Re-landmarked replicates can be considered as similar entities within the morphospace, because 78.07 ± 1.79% (*U*>*UT*=50%) of pattern features are unique to individuals.

DISCUSSION

This study represents the first known use of geometric morphometrics to quantify coat pattern uniqueness in any animal. Individuals of the selected study model (CMZ) have geometrically unique stripe patterns, regardless of resampling error. This suggests that individuals within the population have stripe patterns that are dissimilar enough to rarely be confused for the same individual. We recognized the branches of the four rear torso stripes as being the most geometrically variable components, following allometry and the number of stripes. Geometric morphometrics is well suited to quantify coat pattern variation of homologous pattern features, best visualized by the novel heat maps based on thin-plate splines developed here. This has broad application potential within varied fields of biology, ecology, systematics and even forensics. Specifically here, quantified differences in CMZ stripe patterns provide a baseline of morphological variation for a population (Mountain Zebra National Park; MZNP) for comparison. We recommend a combined approach in which computer vision uniformly spaces landmarks along homologous stripe edges for geometric morphometrics, while scale-invariant feature transform (SIFT) features are automatically identified in variable non-homologous branches and half-stripes.

Stripe features

Previous methods to quantify stripe patterns assumed no allometric changes when using a generic 3D model (Kelly, 2001; Hiby *et al.*, 2009; Reddy & Aravind, 2012). However, disproportionate expansion of animals within their ectoderm with age distorts stripe patterns (Murray, 1988). Shown herein, allometry of the stripe patterns is important to consider when observing changes in the morphology of an animal over time, due to growth and changes in condition. Age-related shape changes occurred in ovenbird (*Seiurus aurocapilla* Linnaeus, 1766) feathers (Sheets *et al.*, 2006), rodent skulls (*Mastomys natalensis* Smith, 1834) (Breno *et al.*, 2011) and turkey beaks (*Meleagris gallopavo* Linnaeus, 1758) (Dalton *et al.*, 2017b), to name just a few cases. Furthermore, fat deposition resulted in shape changes in cichlids (*Cichla temensis* Humboldt, 1821) (Reiss & Grothues, 2015). Future long-term studies should confirm that size related to growth or condition allometrically distort coat patterns that were formed embryonically. Evidence suggested that properties of the coat pattern could indicate individual genetic and developmental condition (Pérez-Rodríguez *et al.*, 2017).

During embryogenesis, natural pattern formation is ineffective at reproducing the number of components (Lange *et al.*, 2018). In this case, CMZ torso stripes vary in number between

nine and 12. In human development, varied numbers of digits are fairly common, owing to changes in distributions of morphogenic activators and inhibitors (Raspopovic *et al.*, 2014). The variation in the number of whole stripes is similarly affected. Although torso stripes past nine were not included, they are accounted for in the curvature of the seventh to ninth torso stripes. Unlike certain fish species, which gained stripes with age and regenerated stripes independent of a predefined pattern (Kondo & Asai, 1995; Yamaguchi *et al.*, 2007), stripes of mammalian coats are fixed in number. Thus, their geometric influence is a reliable predictor of morphological differences between individuals.

Internal shapes of the branching torso stripes and grid-iron pattern are not accounted for here. However, the extent of branching in wing venation of black flies (Diptera: Simulidae) has been inferred from landmarking around branching regions (Pepinelli *et al.*, 2013). Similarly, the external size and shape of CMZ grid-iron patterns, branches and half-stripes, influence the widening and spacing of stripes, shown to be variable in this study. This still provides some quantitative value to individual differences. Shape changes in a stripe feature affect small compensatory changes across numerous features or a large change in an adjacent stripe. The grid-iron extends over both left and right sides of the body and was difficult to scan entirely, thus reducing our grid-iron pattern sample size to statistical infeasibility. The grid-iron pattern may be useful to consider for drone imagery above conscious wild animals.

Of the total pattern variation, more than half occurs due to differences in torso stripe number, branching, incomplete stripes and allometry; measurable without geometric morphometrics. Most pattern variation occurs at the branches of the three rear torso stripes and allometric shape changes. The remaining variation is due to shape variation only feasibly quantifiable by geometric morphometrics. This includes: curvature and roundness, especially at the lowest rump stripe; relative width and length of the torso stripes; external branch shape; and other aspects that are inherent to shape. Patterns are, therefore, not merely amorphous collections of qualitative insights, they also have an indubitable quantitative basis to them.

Unlike current 2D, deep/machine learning (Tharwat *et al.*, 2017) or feature extraction (Crall *et al.*, 2013) methods, our approach provides 3D data that would otherwise be lost around the curved edges of the animal in the field of view and to perspective skews (Lahiri *et al.*, 2011). Herein, we collect such data through triangulation between multiple angled photographs. We do not dissuade the use of deep/machine learning and 2D feature extraction approaches for rapid identification but, where available, quantifiable 3D data should not be ignored. This 3D data considers the overall dimensions and shape of the animal to provide undistorted coat patterns that are not only useful for identification, but also for accurate phenotypic monitoring. Furthermore, this approach may be automated through colour-based edge detection (Huang, 2019) and landmark placement along edges. The potential application to monitor phenotypic variation is especially important for the genetically constrained species/subspecies such as CMZ.

Future studies

Asymmetry is an intrinsic factor affecting morphological variation derived from one side. Reddy & Aravind (2012) quantified asymmetry between left and right sides of plains zebra (*Equus quagga* Boddaert, 1785) using a short-time Fourier transform (STFT) projection technique. Plains zebra sides were 17% to 28% unique to one another (Reddy & Aravind, 2012) compared to 78% uniqueness between individuals, an acceptable degree of asymmetry. In this study, only the left or right side of individuals was analysed. However, it is

inadvisable to extensively shift zebra once immobilized, to prevent epidermal damage and intestinal complications (SANParks standard operating procedure 2015). We also could not subset for left and right orientations as statistical power would be impacted. Future studies should quantify the extent of these asymmetrical differences using geometric morphometrics. Furthermore, quantifying pattern distortion from skin cell expansion and migration over time using photogrammetry could provide avenues for cancer research aided by CMZ's dense striping (Marais *et al.*, 2007; Gan *et al.*, 2013).

We modelled immobilized individuals using a single or small set of cameras. However, research is underway to photogrammetrically model moving individuals with ten to 32 cameras (Postma & De Bruyn, 2015). Cameras are pointed inwards towards a central scene, such as a bush path, and triggered simultaneously through motion detection, to essentially freeze a moving animal in time and space (Waite *et al.*, 2007; Postma & de Bruyn, 2015). This approach applies to volume and curvilinear measurements but could easily be extended to surface features, given enough coverage to retain surface colour information (Bot & Irschick, 2019). Applying this approach to large, free-ranging, terrestrial animals would solve the issue of asymmetry, removes the need for immobilization and thus removes error associated with slight movements during immobilization. Furthermore, one could produce a 3D model using video frames (Burghardt & Campbell, 2007) but ignore variable 3D dimensions in the model itself. The automatic and non-invasive nature of such approaches allows one to attain larger sample sizes for cross-sectional studies or long-term temporal studies of individuals over time, without stress to the animal. In this case, to understand how stripe patterns may vary over large spatial (e.g. across isolated populations) or temporal (e.g. with growth) scales.

It is of management and conservation interest how, for example, the stripe patterns of CMZ populations vary. Morphological baselines of founder populations need to be established before comparisons can be made with derivative populations; where mixing of genes, and possibly resultant stripe patterns, occur. The comparison can be extended towards HMZ to validate their supposed sparser rump and shorter torso stripes (Novellie *et al.*, 2002; Groves & Bell, 2004) using geometric morphometrics. Inter-species (*E. quagga* and *E. grevyi* Oustalet, 1882) comparisons require a geometric morphometric approach wherein homologous stripe components are identified across species and validated before pilot studies of landmark placement are undertaken. These methods could be important for traceability to a population of origin alongside quantitative genetics by quantifying differences in population stripe characteristics and preventing hybridization between species and subspecies. Traceability of stripe patterns could allow us to attribute, for example, an incorrectly translocated individual to its population of origin.

Whether this approach can be extended to non-zebra taxa requires evaluation. Finding homology between spots or dapples could be difficult, but the placement of these features relative to internal anatomy or external curvature guides correspondences. Are spots just discontinuous stripes? We do not see spots in zebra due to the saturation of melanistic activators, which is often seen on the tapered ends of spotted cat tails (Murray, 1988; Ball, 2001). Using this knowledge, detailed investigation is required on whether spots line up along, what could be, branching ridges of melanistic activation. This could guide future geometric morphometrics of homologous lines of spots.

CONCLUSION

Coat similarity is a measure of morphological similarity for use in systematics, forensics, identification and phenotypic monitoring. Previous studies have used qualitative and quantitative measures of coat similarity for individual identification. However, our study provides useful quantification of shape differences and variation that includes not only locally distinct points, but also 3D geometric aspects that have previously been ignored. This more holistic approach to quantifying pattern differences could provide more accurate measures of morphological variation. Additionally, geometric morphometrics of the surface provides the potential to study the effect of skin cell migration and expansion, and quantify condition. Geometric morphometrics works within a 3D photogrammetric framework, allowing for synchronized volume, surface and linear estimates; and now includes relative differences in coat geometry along surfaces for a broad range of studies requiring morphological variation.

SUPPORTING INFORMATION

S1. We illustrate the camera array used, angles of the outermost cameras on GoPro Hero4 mounts (dashed lines) from the side (A), the aluminum grid and handle (solid lines) from the top (B), and its application (C). The ideal angle for the outermost cameras is ~ 45° but does not need to be exact and can be adjusted for the situation. The configuration merely help quickly gain coverage of the photographed animals (D) and is not necessary for the approach. Black boxes represent the angles that were photographed.

S2. Full resolution heat map GIFs illustrating regions of shape variation along the first 10 principal axes (PCs; numbered). Redness (255, 200, 100) of red-green-blue (RGB) values was constrained to regions with the top 1%, 5% and 10% of shape variation along the principal axes, respectively.

Appendix 1. The most parsimonious models from stepwise AIC model selection for each principal component (PC). The Akaike's Information Criteria was corrected for small sample size (AICc). The variation of each PC explained by the model (R^2) and cumulative shape variation explained by the PC was reported. Models that violated the linear model assumptions of no kurtosis, normally distributed variance or homoscedasticity were ignored (*). Negative coefficients for predictors are illustrated with minus superscripts (–). Interactions between predictors, simultaneous but non-additive effects on the response, are illustrated using a colon (:). Predictor variables include branching of the first to ninth torso stripe (B1–9), branching of half stripes in front of the grid-iron pattern (HG) and first to eight torso stripes (H1–8), size and the number of torso stripes (Stripes). Model formulae should be viewed alongside models warped for shape along principal components.

Appendix 2. Heat maps illustrating regions of shape variation along principal axes (PCs; numbered). Heat maps were plotted on models warped (*geomorph* package) to illustrate minimum values of principal components. RGB redness (255, 200, 100) was constrained to regions with the top 1%, 5% and 10% of shape variation along the principal axes, respectively.

ACKNOWLEDGEMENTS

Field assistance by Nico Lübcker is acknowledged. We thank Dean Adams and Antoine Marchal for assistance regarding the use of geometric morphometrics. Megan Coetzee and Roz Prinsloo commented on earlier drafts. SANParks Veterinary Wildlife services and Mountain Zebra National Park management, especially Lourens de Lange, Angela Bruns, Rudi Williams and David Zimmermann allowed us to join capture events for which a SANParks research permit (DEBR-PJN/2018-016) was attained. The Technology Innovation Agency funded the study.

REFERENCES

Adams DC, Otárola-Castillo E. 2013. Geomorph: an R package for the collection and analysis of geometric morphometric shape data. *Methods in Ecology and Evolution* 4: 393 – 399.

Ball P. 2001. *The self-made tapestry: pattern formation in nature*. New York: Oxford University Press.

Bandeira LN, Alexandrino J, Haddad CFB, Thomé MTC. 2017. Geographical variation in head shape of a Neotropical group of toads: the role of physical environment and relatedness. *Zoological Journal of the Linnean Society* 179: 354 – 376.

Bignon O, Baylac M, Vigne J-D. 2005. Geometric morphometrics and the population diversity of Late Glacial horses in western Europe (*Equus caballus arcelini*): phylogeographic and anthropological implications. *Journal of Archaeological Science* 32: 375 – 391.

Bookstein FL. 1996. Combining the tools of geometric morphometrics. In: Marcus LF, Corti M, Loy A, Naylor GJP, Slice DE, eds. *Advances in morphometrics*. New York: Plenum, 131 – 151.

Bot JA, Irschick DJ. 2019. Using 3D photogrammetry to create open-access models of live animals: 2D and 3D software solutions. In: Grayburn J, Lischer-Katz Z, Golubiewski-Davis K, Ikeshoji-Orlati V, eds. *3D/CR in the Academic Library: emerging practices and trends*. Arlington: Council on Library and Information Resources, 54 – 72.

Breno M, Leirs H, Van Dongen S. 2011. Traditional and geometric morphometrics for studying skull morphology during growth in *Mastomys natalensis* (Rodentia: Muridae). *Journal of Mammalogy* 92: 1395 – 1406.

Burghardt T, Campbell N. 2007. Individual animal identification using visual biometrics on deformable coat-patterns. *International Conference on Computer Vision Systems* (ICVS) 5: 1–10.

Cheema GS, Anand S. 2017. Automatic detection and recognition of individuals in patterned species. In: Atun Y, Das K, Mielikäinen T, Malerba D, Stefanowski J, Read J, Žitnik M, Ceci M, Džeroski S. eds. *Machine learning and knowledge discovery in databases. Cham*: Springer, 27 – 38.

Cignoni P, Callieri M, Corsini M, Dellepiane M, Ganovelli F, Ranzuglia G. 2008. MeshLab: an open source mesh processing tool. E*urographics Italian Chapter Conference* Salerno: The Eurographics Association, 129 – 136.

Crall JP, Stewart CV, Berger-Wolf TY, Rubenstein DI. 2013. HotSpotter – patterned species instance recognition. IEEE Workshop on Applications of Computer Vision (WACV). Washington, DC: IEEE computer society, 230 – 237.

Dalton DL, Zimmermann D, Mnisi C, Novellie P, Hrabar H, Kotzé A, Dalton DL, Zimmermann D, Mnisi C, Taplin M, Novellie P, Hrabar H. 2017b. Hiding in plain sight: evidence of hybridization between Cape mountain zebra (*Equus zebra zebra*) and plains zebra (*Equus quagga burchelli*). *African Journal of Wildlife Research* 47: 59 – 64.

Dalton HA, Wood BJ, Widowski TM, et al. 2017. An analysis of beak shape variation in two ages of domestic turkeys (*Meleagris gallopavo*) using landmark-based geometric morphometrics. *PLoS One* 12: e0185159.

Davis MA, Douglas MR, Collyer ML, Douglas ME. 2016. Deconstructing a species-complex: geometric morphometric and molecular analyses define species in the western rattlesnake (*Crotalus viridis*). *PLoS One* 11: e0146166.

Eos Systems Inc. 2017. *Photomodeler Scanner*.

Fisher RA. 1926. The arrangement of field experiments. *Journal of the Ministry of Agriculture in Great Britain* 33: 1469 – 1472.

Gower JC. 1975. Generalized procrustes analysis. Psychometrika 40: 33 – 51.

Groves CP, Bell CH. 2004. New investigations on the taxonomy of the zebras genus *Equus*, subgenus *Hippotigris. Mammalian Biology* 69: 182 – 196

Gan X, Wang C, Patel M, Kreutz B, Zhou M, Kozasa T, Wu D. 2013. Different RAF protein kinases mediate different signaling pathways to stimulate E3 ligase RFFL gene expression in cell migration regulation. *The Journal of Biological Chemistry* 288: 33978–33984.

Henneke D. 2011. Body conditioning score. In: Wilson DA, eds. *Clinical Veterinary Advisor: The Horse.* St. Louis: Elsevier Saunders, 675–677.

Hiby L, Lovell P, Patil N, et al. 2009. A tiger cannot change its stripes: using a three-dimensional model to match images of living tigers and tiger skins. *Biology letters* 5: 383 – 386.

Hrabar H, Birss C, Peinke D, King S, Novellie P, Kerley G, Child M. 2016. *Equus zebra zebra* – Cape mountain zebra. In: Child MF, Roxburgh L, Do Linh San E, Raimondo D, Davies-Mostert HT, eds. *The red list of mammals of South Africa, Lesotho and Swaziland.* Johannesburg : South African National Biodiversity Institute and Endangered Wildlife Trust.

Huang YJ. 2019. Color-based edge detection on mesh surface. *SIGGRAPH Asia 2019 Posters*. New York: ACM, 2

Jansky KJ, Schubert BW, Wallace SC, Mead JI. 2013. *Identifying Myotis species using geometric morphometrics and its implications for the fossil record and conservation*. Unpublished M.Sc. Thesis, East Tennessee State University.

Kelly MJ. 2001. Computer-aided photograph matching in studies using individual identification: an example from Serengeti cheetahs. *Journal of Mammalogy* 82: 440 – 449.

Kondo S, Asal R. 1995. A reaction-diffusion wave on the skin of the marine angelfish Pomacanthus. *Nature* 376: 765 – 768.

Lahiri M, Tantipathananandh C, Warungu R, Rubenstein DI, Berger-Wolf TY. 2011. Biometric animal databases from field photographs: identification of individual zebra in the wild. *Proceedings of the 1st ACM international conference on multimedia retrieval (ICMR)* 6: 1 – 8.

Lange A, Nemeschkal HL, Müller GB. 2018. A threshold model for polydactyly. *Progress in Biophysics and Molecular Biology* 137: 1 – 11.

Luceño AJM, Torres MAJ, Tabugo SR, Demayo CG. 2013. Describing the body shapes of three populations of *Sardinella fimbriata* (Valenciennes, 1847) from Mindanao Island, Philippines using relative warp analysis. *Annals of Biological Research* 4: 29 – 39.

Marais HJ, Nel P, Bertschinger HJ, et al. 2007. Prevalence and body distribution of sarcoids in South African Cape mountain zebra (*Equus zebra zebra*). Journal of the South African Veterinary Association 78: 145 – 148.

Marquez F, Robledo J, Penaloza GE, Van der Molen S. 2010. Use of different geometric morphometrics tools for the discrimination of phenotypic stocks of the striped clam *Ameghinomya antiqua* (Veneridae) in north Patagonia, Argentina. *Fisheries Research* 101: 127 – 131.

Mason AD. 2016. *Monitoring individual animals through a collaborative crowdsourcing and citizen science platform*. Unpublished Ph.D. Thesis, University of Surrey.

McGuire JL. 2011. Identifying California Microtus species using geometric morphometrics documents Quaternary geographic range contractions. *Journal of Mammalogy* 92: 1383 – 1394.

de Mendiburu F. 2017. *Agricolae: statistical procedures for agricultural research*. R Package Version 1.1-4.

Miththapala S, Seidensticker J, Phillips LG, Fernando SBU, Smallwood JA. 1989. Identification of individual leopards (*Panthera pardus kotiya*) using spot pattern variation. *Journal of Zoology* (London) 218: 527 – 536.

Murray JD. 1988. How the leopard gets its spots. *Scientific American* 258: 80 – 87.

Norouzzadeh MS, Nguyen A, Kosmala M, Swanson A, Palmer M, Packer C, Clune J. 2018. Automatically identifying, counting, and describing wild animals in camera-trap images with deep learning. *Proceedings of the National Academy of Sciences of the USA* 115: 5716 – 5725.

Novellie P, Lindeque M, Lindeque P, Lloyd P, Koen J. 2002. Status and action plan for the mountain zebra (Equus zebra). In: Moehlman P, ed. *Equids: zebras, asses and horses. Status survey and conservation action plan*. Gland : IUCN, 28 – 42.

Peña E, Slate E. 2006. Global validation of linear models assumptions (gvlma). *Journal of American Statistical Association* 101: 341 – 354.

Penzhorn BL. 1984. A long-term study of social organisation and behaviour of Cape mountain zebras *Equus zebra zebra. Zeitschrift für Tierpsychologie* 64 : 97 – 146.

Penzhorn BL. 1988. *Equus zebra. Mammalian Species* 314: 1 – 7.

Penzhorn BL, Novellie PA. 1991. Some behavioural traits of Cape mountain zebras (Equus zebra zebra) and their implications for the management of a small conservation area. *Applied Animal Behaviour Science* 29: 293 – 299.

Pepinelli M, Spironello M, Currie DC. 2013. Geometric morphometrics as a tool for interpreting evolutionary transitions in the black fly wing (Diptera: Simuliidae). *Zoological Journal of the Linnean Society* 169: 377 – 388.

Pérez-Rodríguez L, Jovani R, Stevens M. 2017. Shape matters: animal colour patterns as signals of individual quality. *Proceedings of the Royal Society B: Biological Sciences* 284: 20162446.

Peterson JCB. 1972. An identification system for zebra (*Equus burchelli, Gray*). *African Journal of Ecology* 10: 59 – 63.

Postma M, De Bruyn PJN. 2015. Automated photogrammetry body mass estimation of large mammals. *6th Annual Diamond Route Research Conference* 6: 6.

Purroy A, Šegvić-Bubić T, Holmes A, et al. 2016. Combined Use of Morphological and Molecular Tools to Resolve Species Mis-Identifications in the Bivalvia The Case of *Glycymeris glycymeris* and *G. pilosa*. *PLoS One* 11: e0162059.

R Core Team. 2018. *R: a language and environment for statistical computing.* Vienna: R Foundation for Statistical Computing.

Raspopovic J, Marcon L, Russo L, et al. 2014. Modeling digits. Digit patterning is controlled by a Bmp-Sox9-Wnt Turing network modulated by morphogen gradients. *Science (New York, N.Y.)* 345: 566 – 570.

Reddy KPK, Aravind R. 2012. Measurement of asymmetry of stripe patterns in animals. *International Conference on Signal Processing and Communications*. Bangalore: IEEE, 1–5.

Reiss P, Grothues TM. 2015. Geometric morphometric analysis of cyclical body shape changes in color pattern variants of *Cichla temensis* Humboldt, 1821 (Perciformes: Cichlidae) demonstrates reproductive energy allocation. *Neotropical Ichthyology* 13: 103 – 112.

Schmieder DA, Benítez HA, Borissov IM, et al. 2015. Bat species comparisons based on external morphology: a test of traditional versus geometric morphometric approaches. *PLoS One* 10: e0127043.

Sheets HD, Covino KM, Panasiewicz JM, et al. 2006. Comparison of geometric morphometric outline methods in the discrimination of age-related differences in feather shape. *Frontiers in Zoology* 3: 15.

Tharwat A, Gaber T, Hassanien AE, Schaefer G, Pan JS. 2017. A fully-automated zebra animal identification approach based on SIFT features. *Advances in Intelligent Systems and Computing* 536: 289 – 297.

Vendrami DP, Obara MT, Gurgel-Gonçalves R, et al. 2017. Wing geometry of Triatoma sordida (Hemiptera: Reduviidae) populations from Brazil. *Infection, Genetics and Evolution: journal of molecular epidemiology and evolutionary genetics in infectious diseases* 49: 17 – 20.

Waite JN, Schrader WJ, Mellish JE, Horning M. 2007. Three-dimensional photogrammetry as a tool for estimating morphometrics and body mass of Steller sea lions (*Eumetopias jubatus*). *Canadian Journal of Fisheries and Aquatic Sciences* 64: 296 – 303.

Wiley DF, Amenta N, Alcantara DA, Delson E, Harcourt-Smith W, Rohlf FJ, John KS. 2005. Evolutionary Morphing. In: Silva CT, Gröller E, Rushmeier HE, eds. *VIS 05. IEEE Visualization.* Minneapolis: IEEE, 431–438.

Wisely SM, Santymire RM, Livieri TM, Mueting SA, Howard J. 2008. Genotypic and phenotypic consequences of reintroduction history in the black-footed ferret (Mustela nigripes). Conservation Genetics 9: 389 – 399

Yamaguchi M, Yoshimoto E, Kondo S. 2007. Pattern regulation in the stripe of zebrafish suggests an underlying dynamic and autonomous mechanism. *Proceedings of the National Academy of Sciences of the United States of America* 104: 4790 – 4793.